Virtual Hopf Precursor of Period-Doubling Route in Directly Modulated Semiconductor Lasers

Yao Huang Kao, *Member, IEEE,* and Hung Tser Lin

***Abstract*—In this paper the noise effects on the period-doubling route in deeply modulated laser diodes were investigated. The dynamics were studied by employing the single-mode rate equations with consideration of Langevin noise. It was identified that the period-doubling event in laser diodes had a virtual Hopf precursor and was enhanced by the existed Langevin noise.**

I. Introduction

NONLINEAR dynamical behaviors have been enthusiastically investigated in a wide variety of physical systems following the discovery of scaling constants in the routes to chaos [1]. At least three scenarios of routes to chaos have been successfully applied to those systems. They are the Feigenbaum, intermittency, and quasi-periodic routes, and are related to the period doubling (PD), saddle node, and Hopf bifurcations, respectively. The routes to chaos in semiconductor lasers have also been intensively studied not only because of theoretical interest, but also for practical purposes, especially in the area of analog modulation in fiber communication [2]. A solitary single-mode semiconductor laser cannot exhibit chaotic behavior because it is fully described by only two independent quantities: the photon density and carrier density. The adding of an additional degree of freedom, i.e., modulation, light injection, or delay feedback, is necessary to allow for the chaotic instability to occur. The aspect of period-doubling route of a laser diode under direct current modulation is the focus of this paper.

Strong current modulation in semiconductor laser diodes has recently received much attention, especially in the area of high-speed short pulse generation and microwave analog fiber-optic transmission [3]–[18]. The output of photon density under such a circumstance clearly exhibits a number of nonlinear phenomena, i.e., harmonic distortion, pulsation, bistability, quasi-periodic and PD routes to chaos, etc. A set of nonlinear rate equations governing the interrelationship between carrier density and photon density have been commonly applied to forecast the relaxation oscillation and bistability [6], [19]. The influences of the nonlinear gain suppression factor, the spontaneous emission factor, and the Auger recombination factor upon the PD phenomenon have also been numerically examined in the rate equations [10]–[13]. The analytic method utilized for predicting the onset point of a PD route has also been previously presented [14], [15]. Despite great efforts, the important role of noise on the dynamics of the routes to chaos is not yet exploited in detail. The output of a CW diode laser actually exhibits a large-amplitude fluctuation with frequencies around the relaxation oscillation resonance [9], [16]. These fluctuations, denoted as Langevin noise, arise from the quantum nature of spontaneous emission and cannot be eliminated in real diode lasers. The effect of the noise sources should be taken into account for the sake of more realistically modeling the dynamical behaviors of laser diodes. In an earlier work [20], the ability of noise to enhance the occurrence of PD has been numerically confirmed. Here, it is further indicated that the noise can act as an important precursor for the occurrence of the PD. This phenomenon is confirmed to be a virtual Hopf bifurcation [21]. Experiments are also performed on a 1.5-μm InGaAsP DFB laser. The strength of high-frequency power for the onset point is forecasted with an extra consideration of parasitic effects. This study will improve our understanding of the period doubling.

The paper is organized as follows. The rate equations are introduced in Section II with the consideration of Langevin noise as well as a fast searching algorithm for the steady-state solutions. A numerical bifurcation diagram in controlled parameter space is presented in Section III, from which a global picture of instability boundaries can be obtained. The explanations of virtual Hopf bifurcation by Floquet theory are also presented. The experimental demonstration of noise-enhancing period-doubling, parasitic effect, and the phenomena of virtual Hopf precursor are described in Section IV. Concluding remarks are summarized in Section V.

II. The Stochastic Rate Equations

With the inclusion of the nonlinear gain suppression effect, the single-mode rate equations for the photon density S and carrier density n can be written as [6], [12]

$$\frac{dn}{dt} = \frac{I(t)}{eV} - \frac{n}{\tau_e} - A(1 - \epsilon_n S)(n - n_0)S + F_n(t)/V \tag{1}$$

Manuscript received November 5, 1992; revised February 8, 1993. This study was supported by the National Science Council, Republic of China, under Contract NSC81-0404-E009-24.

The authors are with the Department of Communication Engineering and the Center of Telecommunication Research, National Chiao-Tung University, Hsin-Chu, Taiwan, 30050, ROC.

IEEE Log Number 9209111.

$$\frac{dS}{dt} = \Gamma A(1 - \epsilon_{nl}S)(n - n_0)S - \frac{S}{\tau_p} + \frac{\Gamma\beta n}{\tau_e} + F_s(t)/V \tag{2}$$

where e is the electron charge; V is the active volume; τ_e and τ_p are the, respective, electron and photon lifetimes; A is the gain constant; n_0 is the carrier density for transparency; Γ is the confinement factor; β is the spontaneous emission factor; and ϵ_{nl} is the nonlinear gain suppression factor. The driving current containing dc and ac terms can be expressed as $I(t) = I_{dc} + I_{ac} \sin(2\pi ft)$ with driving frequency f. F_s and F_n are Langevin noise sources with zero means that, respectively, arise from spontaneous emission and from the discrete nature of the carrier generation and recombination. Under the Markovian assumptions, the Langevin noises satisfy the general relations [22]

$$\langle F_n(t)\, F_n(t')\rangle = V_n^2\delta(t - t') \tag{3}$$

$$\langle F_s(t)\, F_s(t')\rangle = V_s^2\delta(t - t') \tag{4}$$

$$\langle F_n(t)\, F_s(t')\rangle = \gamma_0 V_n V_s \delta(t - t') \tag{5}$$

where V_n and V_s are the respective variances of F_s and F_n. And γ_0 is the correlation coefficient and approaches unity under the single-mode operation condition. The variances are expressed as follows:

$$V_n^2 = I/e + nV/\tau_e + A(1 + \epsilon_{nl})(n + n_0)SV$$

$$V_s^2 = SV/\tau_p + \Gamma A(1 + \epsilon_{nl}S)(n + n_0)SV + \Gamma A\beta nV/\tau_e$$

$$V_nV_s = -\{\Gamma A\beta nV/\tau e + \Gamma A(1 + \epsilon_{nl}S)(n + n_0)SV\}.$$

Basically, the behavior of rate equations is similar to that in a parallel underdamped oscillator under the small-signal operation [19]. Thus some of the inherent properties of the lasers can be realized from the relaxation-oscillation frequency f_r and the damping factor η given by

$$f_r = \frac{1}{2\pi}\left(\frac{\Gamma A}{eV}\right)^{1/2}(I_{dc} - I_{th})^{1/2} \tag{6}$$

$$\eta = (1/\tau_e + AS_t + S_t\epsilon_{nl}/\tau_p + \beta\Gamma I_{th}/eVS_t)/4\pi f_r \tag{7}$$

where

$$I_{th} = eV[n_0 + (\Gamma A\tau_p)^{-1}]/\tau_e$$

$$S_t = \Gamma\tau_p(I_{dc} - I_{th})/eV.$$

Generally, the order of the damping factor is around 0.1 for InGaAsP laser and can be taken as the underdamping case. The peak width in the frequency response Δf is about $2\eta f_r$. It means that the line shape of the noise bump at the dc case can be easily predicted from these two factors.

The photon density and carrier density in (1) and (2) are further normalized for numerical purposes by defining $P = S/S_0$ and $N = n/n_{th}$ with constant S_0 and $\Gamma(\tau_p/\tau_e)n_{th}$ and the threshold carrier density $n_{th} = \tau_e I_{th}/eV$. The rate equations then become [20]

$$\frac{dN}{dt} = \frac{1}{\tau_e}\left(\frac{I(t)}{I_{th}} - N - \frac{N - \delta}{1 - \delta}(1 - \epsilon P)P\right) + F_n' \tag{8}$$

$$\frac{dP}{dt} = \frac{1}{\tau_p}\left(\frac{N - \delta}{1 - \delta}(1 - \epsilon P)P - P + \beta N\right) + F_s' \tag{9}$$

where $F_n' = F_n/(n_{th}V)$, $F_s' = F_s/(S_0V)$, the constants $\delta = n_0/n_{th}$ and $\epsilon = \epsilon_{nl}S_0$. The fourth-order Runge-Kutta algorithm with time step δt and the FFT processor are employed here for finding the time evolution and frequency spectrum of the output photon density, from which the influences on the bistability and PD can be identified. The time interval Δt is chosen here to be $\Delta t = T/128$, where T is the period of the driving current. This ascertains that the noise spectrum is approximately white within $2f$ which is of interest in the simulation. The computations have been detailed in [20] with an error of less than approximately 1 dB.

For the sake of comparison, the typical values of parameters are chosen as $\tau_p = 6$ ps, $\tau_e = 3$ ns, $\beta = 5 \times 10^{-5}$, and $\delta = 0.692$ as identical to [10] and [12]. The normalized dc bias and ac modulated currents are defined as $I_b = I_{dc}/I_{th}$ and $m = I_{ac}/I_{th}$; m is also denoted as the modulation index. The modulation frequency f and the modulation index m are varied during the simulation with I_b at a fixed value. The relaxation oscillation frequency f_r, approximately equal to 1.512 GHz in the observed case, can serve as a guidepost during searching for the various dynamical behaviors within the interesting frequency range.

The transitions are generally able to be identified from the quantitative change of the time evolution, phase portrait (P, N) and its Fourier spectra. Besides that, transitions located in the periodically forced systems, as in the observed case, can also be identified from the stroboscopically sampled data $(P(l), N(l))$ at $t = 2l\pi/\omega$, where l is an integer. For instance, a limited cycle in the phase space is only equivalent to a fixed point. The transitions of a limit cycle can, therefore, be inferred from the variations of the corresponding fixed point. This reduces the solutions to a two-dimensional set. From the set an iterative map P_Σ can be defined as $P_\Sigma(P(l), N(l)) = (P(l + 1), N(l + 1))$. A fixed point thus has the property of $P_\Sigma(P(l), N(l)) = (P(l), N(l))$ and is denoted as $(P^*(l), N^*(l))$. In computations, both the stable and unstable fixed points can be found by iterating from an initial guess X^0 using the relation of

$$X^{i+1} = X^i - (DH(X^i))^{-1}H(X^i)$$

where $H(X) \equiv X - P_\Sigma(X)$, DH is the Jacobian of function H, and the superscript i indicates the iteration count [23]. Not only the onset point of instability but also the type of local bifurcation can be determined from the eigenvalue of the Jacobian $DP_\Sigma(X^*)$, i.e., Floquet multipliers. The results are detailed in the following sections.

III. Numerical Results

A. Thresholds of Period Doubling

The possible transitions related to the less damping case with $\epsilon = 0$ ($\eta \cong 0.0469$) and without Langevin noise in (8) and (9) are first examined for the sake of realizing the rich variety of dynamical behavior primarily originating from nonlinear instability. The dynamical behaviors of output photon density include multiple and submultiple spiking, a period-doubling route to chaos, and hysteresis, whereas the self-pulsation phenomenon is not observed. The transition boundaries in terms of driving frequency and modulation index are depicted in Fig. 1 for a typical case with a dc bias current of $I_b = 1.5$. A global view of possible transitions in the rate equations (8), (9) is provided here through means of this figure. The relevant features of the transitions are detailed in [24]. The overall output photon density becomes spiky if the ac current is increased to reach the minimum of the current swing approach to the threshold current level, i.e., $m \simeq 0.5$. The output contains multiple spikes for $f < f_r$ and submultiple spikes for $f > f_r$. The threshold PD_1 of period doubling with frequency variation from f_r to $2f_r$ actually possesses the minimum required ac current and is conjectured to be the most expected transition in the real experiment. The threshold $HS_{1/2}$ of hysteresis, meanwhile, overlaps with the PD_1. Two types of period doubling can be therefore observed. Both of them contain half-subharmonic components in the frequency spectrum and cannot be solely differentiated from the spectra. One is the normal type of period doubling and is unrelated to the hysteresis. The height of the two adjacent spikes of the output waveform is shown in Fig. 2(a) to be different, and is denoted as type I. It can be found with parameters away from the overlap section of curve $HC_{1/2}$. The other is shown in Fig. 2(b) to reveal only one spike within two external periods, and is denoted as type II. Type-II period doubling often occurs accompanied by hysteresis and can be found in Fig. 1 with the parameters on the overlapped section of curves PD_1 and $HS_{1/2}$. The variations of PD_1 under different combinations of ϵ and noise are focused on in the following.

The variations of the U-shaped threshold at the heavier damped case with $\epsilon = 0.01$ ($\eta \cong 0.0908$) are next examined as used in InGaAsP laser diode, and with a noise effect. The U-shaped threshold of PD is detailed in Fig. 3 to be lifted upward for $\epsilon = 0.01$. A stronger ac current is indicated by this occurrence to be required for attaining the period doubling. The phenomenon of hysteresis, meanwhile, disappears, i.e., the type II PD is not observed.

The noise effect on PD is subsequently examined on the basis of the above results. The laser output is well known to actually reveal a noise bump whose peak frequency is centered around the relaxation oscillation frequency without ac current as shown in Fig. 4(a). The linewidth (HMFW) of the bump is roughly determined by $\Delta f = 2\eta f_r (\cong 275$ MHz). The fluctuation then increases in amplitude and its peak frequency shifts gradually toward $f/2$, e.g., the subharmonic of the modulation frequency, as the modulation index increases to a certain level ($m = 0.5$ and 0.75 in Fig. 4(b) and (c)). Note that the width of the bump has no obvious change. The laser diodes could be taken as a tunable amplifier with Langevin noise as a wideband small ac signal. The tunability of the bump is controlled by the amplitude of an external ac current. The PD

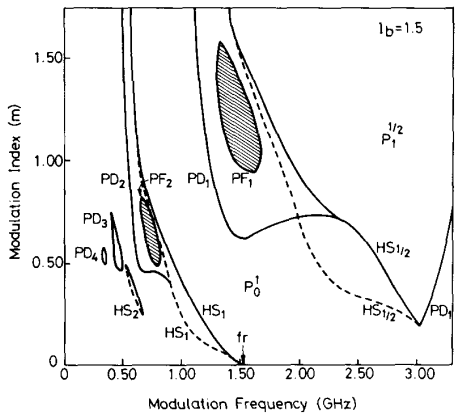

Fig. 1. Two-dimensional state diagram with modulation index and modulation frequency as controlled variables at fixed dc bias $I_b = 1.5$. Curve HS_m is the boundary of hysteresis jump of the mth spiking state; the section with broken line denotes the downward jump. Curves PD_m and PF_m are the boundaries of period doubling and period-four of the mth spiking state, respectively.

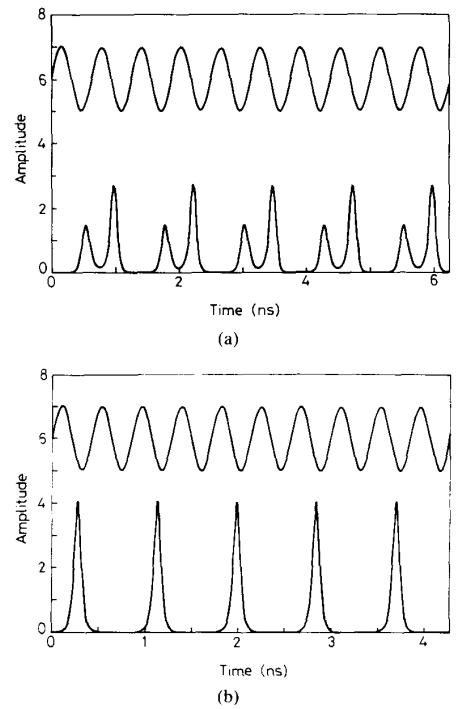

Fig. 2. (a) Time evolution with $f = 1.6$ GHz and $m = 0.85$. (b) Time evolution with $f = 2.34$ GHz and $m = 0.75$.

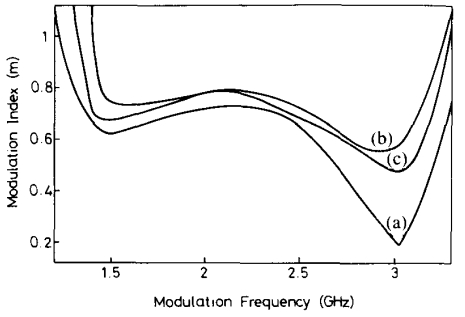

Fig. 3. U-shaped state diagram with (a) $\epsilon = 0.0$, (b) $\epsilon = 0.01$, and (c) $\epsilon = 0.01$ and Langevin noise.

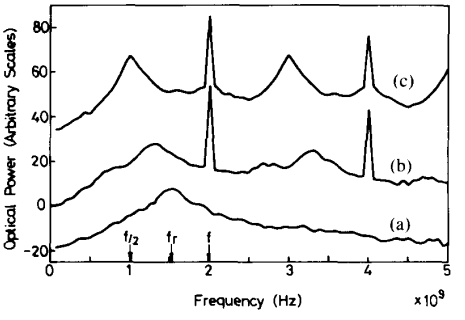

Fig. 4. The Fourier spectra at $f = 2$ GHz, $I_b = 1.5$ and (a) $m = 0$, (b) $m = 0.5$, and (c) $m = 0.75$.

behavior is then consequently observed. The reduced threshold for PD with noise involved is shown in the comparison of curves b and c in Fig. 3. The most significant reduction occurs at $f \cong 2f_r$. When the external force is set to two times the relaxation oscillation, we realize that the noise bump instantly pulled toward $f/2$ and enhances the emergence of period doubling. No obvious change in the threshold is found with frequency around the middle region since the effect of pulling ceases as the subharmonic $f/2$ is far away from the relaxation frequency.

B. Noise Precursor

The Floquet theory is employed here for examining the intensity spectrum [21] so as to further explore the features of bifurcation of the ac-pumped laser diode. Equations (8) and (9) can be rewritten for the sake of brevity as

$$\dot{X} = F(X; m) + \xi, \qquad X \in R^N \tag{10}$$

where modulation index m is the observed controlled parameter, and ξ is white noise

$$\langle \xi(t) \rangle = 0 \qquad \langle \xi_i(t)\xi_j(t + \tau) \rangle = \kappa_{ij}\delta(t) \tag{11}$$

κ_{ij} is the noise strength. X_0 is allowed to be a periodic solution of the noise-free system with $X_0(t + T) = X_0(t)$. For small deviations $\eta_d = X - X_0$, (10) can be linearized about X_0 so as to obtain

$$\eta_d = [DF(X_0; m)]\, \eta_d + \xi \tag{12}$$

where Jacobian DF is the matrix of periodic functions

$$(DF)_{ij} = \left.\frac{\partial F_i}{\partial X_j}\right|_{X = X_0} \tag{13}$$

Equation (12) is linear with periodic coefficients and an exact solution can be obtained using the Floquet theory. The external noise functions as a factor in kicking the system away from the limit cycle. The fixed point X^* can be first computed and then the Floquet multipliers μ can be obtained from the eigenvalues of the Jacobin $DP_\Sigma(X^*)$. The period in the coefficients is normalized for the sake of convenience to have 2π period; the solution φ in (12) then satisfies the property of

$$\varphi(t + T) = \mu\varphi(t). \tag{14}$$

The stability of the basic solution X_0 can then be identified from the criterion with μ lying inside the unit circle, i.e., $|\mu| \leq 1$. An instability occurs with μ crossing outside the unit circle. The period-doubling bifurcation occurs when a single μ is crossing the unit circle at -1 and the Hopf bifurcation occurs when a pair of μ and μ^* are moving across a circle. Moreover, the noise precursor of the intensity spectrum has been indicated to have a closed relation with μ value [21]. If $\mu = e^{-\epsilon'} e^{i\theta} \cong (1 - \epsilon')e^{i\theta}$, the size and shape of the precursor are determined by ϵ' and the noise strength κ as defined in (11); their position is, meanwhile, determined by the angle Θ, i.e., peak high proportional to κ/ϵ', peak width proportional to ϵ', and peak frequency shift proportional to Θ. The noise spectrum can therefore be characterized from the site of Floquet multiplier within the unit circle plane.

The calculated locus of Floquet multiplier at $I_b = 1.5$ is shown in Fig. 5 with a varying modulation index m under three different pumping frequencies of $f = 1.5$, 2, and 3 GHz. The Floquet multiplier pairs $\mu\mu^*$ are initially located near by $\Theta \cong \pm 0°$ for $f = 1.5$ GHz, near by $\Theta \cong 90°$ and 270° for $f = 2$ GHz, and near by $\pm 180°$ at $f = 3$ GHz. The critical modulation index m_c defined with the complex pair of multiplier μ merging at $\epsilon' - 1$ are a respective $m_c \cong 0.645$, 0.725, and 0.005 for $f = 1.5$, 2, and 3 GHz. Below the critical index the multiplier appears as a complex pair, the shape of noise bump maintains a fixed width same as that without modulation. Above the critical index the complex pair merge and split into two negative real numbers and one of them approaches toward -1. In such a case, the spectrum becomes narrower and narrower as the excitation reaches closer and closer to the onset point of period doubling. Moreover, at $f = 3$ GHz μm is located near $-1 + \epsilon$ initially, and PD easily occurs. This is another reason why the onset point of PD shown in Fig. 3 is to be nearly the lowest one at $f = 3$ GHz. Note that the above transition process is referred to as virtual Hopf bifurcation, because the complex conjugate pair lies initially very close to the unit circle, a situation that generally occurs just before the onset of a Hopf bifurcation. However, instead of exiting the unit circle, the multipliers move along the circle $|\mu| = 1 - \epsilon'$, until they

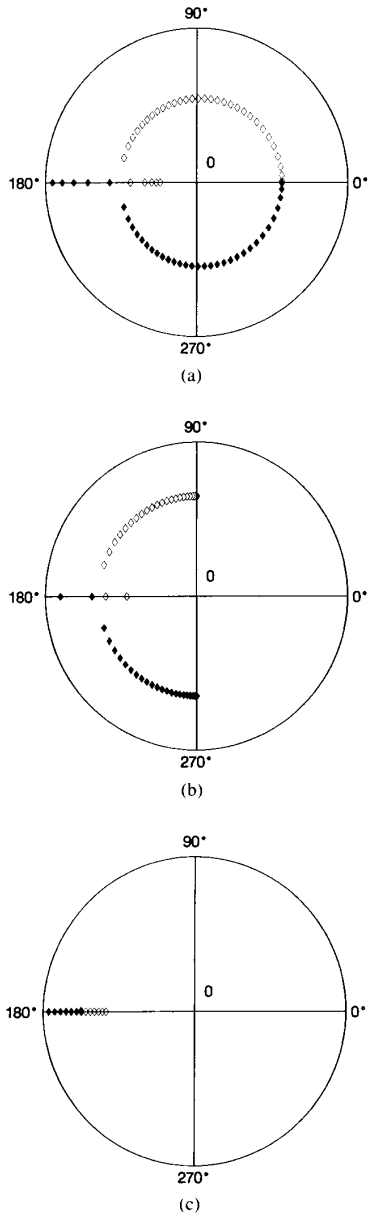

Fig. 5. The calculated locus of Floquet multiplier scanning the modulation index m with I_b = 1.5 and (a) f = 1.5 GHz, (b) f = 2 GHz, and (c) f = 3 GHz.

meet on the negative real axis. At all events, the Langevin noise forms a noise precursor in the spectrum and can enhance the threshold of period doubling.

IV. Measurement Results

The predicted thresholds are also compared with the experimental results of a commercially available ridge-guide DFB laser. The laser diode used in the observed experiment is an InGaAsP–InP DFB ridge waveguide type with a wavelength at 1.55 μm (STC LYC-M2-11). Its threshold current I_{th} at 20°C is 36.5 mA. The relaxation oscillation frequency f_r varies between 1 and 4 GHz for bias current I_{dc} between 37 and 60 mA. Obtaining the proper values of the coefficients in (1) and (2) and the parasitic effects are essential for the sake of comparison with the real experiments. In the observed case the major contributions in the parasitic parameters, below 3 GHz, come from the resistance R_s in series with the active region and the shunt capacitance C_s between the metal contact [18]. The values are as follows: $n_0 = 1.0 \times 10^{24}/\text{m}^3$, $V = 0.2 \times 5 \times 250\ \mu\text{m}^3$, $\Gamma = 0.3$, $A = 3.2 \times 10^{-12}\ \text{m}^3/\text{s}$, $\tau_p = 1$ ps, $\tau_e = 2.27$ ns, $\beta = 2 \times 10^{-4}$, $\epsilon_{nl} = 6.7 \times 10^{-23}\ \text{m}^3$ with a bias current of 39 mA. The time constant R_sC_s is approximately equal to 140 ps with -3 dB frequency at 1.137 GHz. These two elements function as a low-pass filter for shunting a part of the RF current going into the active region if the excitation frequency exceeds the corner one. These parameters have been satisfactorily confirmed by verifying the second-harmonic distortions [18]. The thresholds of PD are examined in the following by thorough usage of these parameters and are put into comparison with the experimental results.

The first onset of PD with a bias I_{dc} = 39 mA near the threshold is thus investigated here. The corresponding relaxation oscillation frequency is $f_r \cong 1.3558$ GHz and the damping factor η is about equal to 0.259. The strength of ac current is expressed in terms of dBm for the sake of convenience. With the diode connected through a bias-T to the 50-Ω RF signal generator, the amplitude I_{ac} related to dBm can be expressed as I_{ac} (mA) $\cong 12.65 \times 10^{\text{dBm}/20}$ under the approximation with dynamical resistor of laser diode much less than 50 Ω. The measured threshold in the RF power and frequency space as a V shape (curve b), rather than a U shape (curve a) is shown in Fig. 6. Parasitic effects R_s C_s should notably be taken into account, as compared to the real experiment. The threshold current I'_{ac} in real experiment should therefore be larger than that predicted above. The relationship between I'_{ac} and I_{ac} in (1) can be expressed as $I'_{ac} \cong I_{ac}[(1 + R_s/50)^2 + (2\pi f R_s C_s)^2]^{1/2}$ under the assumption that the impedance of the active region is significantly less than R_s. The required threshold values are accordingly lifted up as illustrated in curve c of Fig. 6, which seems to be in good agreement with the measured value as curve b of Fig. 6. Only a small amount of RF power is required for generating the PD if the driving frequency is near $2f_r$, whereas, the noise-enhanced effect dies out when the excitation frequency is too far away from two times of the relaxation frequency. This therefore requires stronger RF power to reach the thresholds. The exhibition of PD by amplitude scanning with a frequency at 2.2 GHz near $2f_r$ is demonstrated in Fig. 7(a)–(c) and by frequency scanning with fixed RF power are shown in Fig. 7(d)–(f). In frequency scanning only Fig. 7(e) with frequency at 1.85 GHz near $2f_r$ reveals the PD.

The threshold without noise and parasitic effects in (1) and (2) is also calculated for the sake of comparison. The PD phenomenon is unfortunately not observed with ac

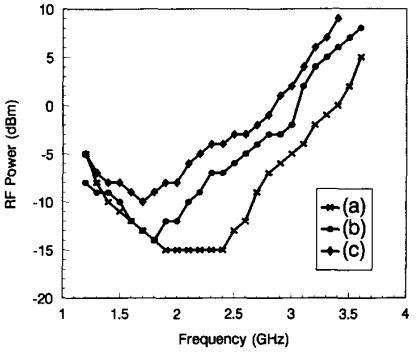

Fig. 6. Two-dimensional state diagram describing the onset of PD in the RF power and frequency space for I_{dc} = 39 mA. Curve a is the calculated result with noise and without R_sC_s; curve b is the measured results; and curve c is with noise and R_sC_s.

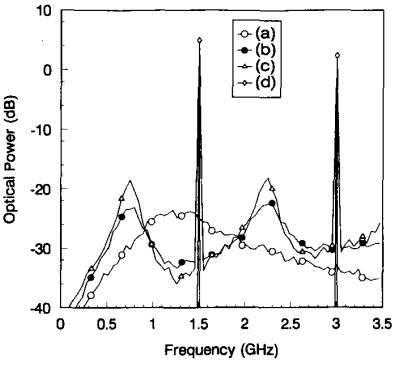

Fig. 8. The calculated Fourier spectra with f_1 = 1.5 GHz and (a) no RF power, (b) RF power = −2 dBm, (c) RF power = 5 dBm, and (d) RF power = 5 dBm but without noise perturbation at f_1 = 1.5 GHz.

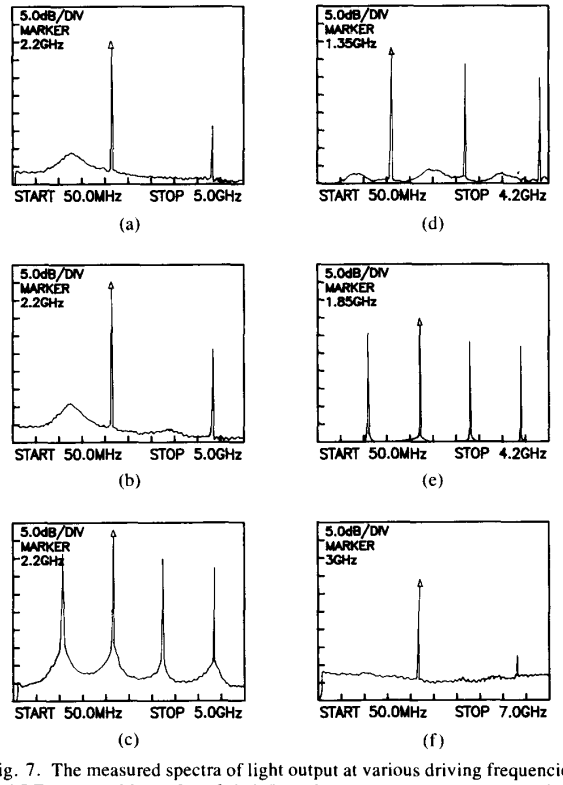

Fig. 7. The measured spectra of light output at various driving frequencies and RF power with (a) f_1 = 2.2 GHz and power = −10.7 dBm, (b) f_1 = 2.2 GHz and power = −6.55 dBm, (c) f_1 = 2.2 GHz and power = 1.9 dBm, (d) f_1 = 1.35 GHz and power = +1.9 dBm, (e) f_1 = 1.85 GHz and power = +1.9 dBm, and (f) f_1 = 3.0 GHz and power = +1.9 dBm.

signal strength up to +10 dBm in the whole frequency range, whereas the situation totally changes when the Langevin noises are taken into account. The onset is identified here as the emergence of a half-subharmonic signal out of the noise level the same as in the experiment. Only an intrinsic noise bump shown in curve a of Fig. 8 exists around f_r in the output spectrum without the RF signal. The noise level is then increased with the peak frequency shifting toward a lower frequency as modulation is increased with frequency f between f_r and $2f_r$. The respective cases are shown as curves b and c of Fig. 8 with RF power = −2 and +5 dBm, at f = 1.5 GHz. The symptom of PD occurs whenever the maximum of the noise bump is tuned to approach the subharmonic component $f_1/2$ by increasing the ac current, whereas, no subharmonic signal is illustrated in curve d when the noise is removed. This implies that the occurrence of PD can be indeed enhanced by the noise. The moving procedure is evidenced in Fig. 7(a)–(c). Indeed, the virtual Hopf bifurcation is observed.

V. Conclusion

The noise effect on the period doubling of a current-modulated semiconductor laser was extensively investigated in this paper. The most remarkable region of period doubling with the U-shaped threshold was found in the frequency interval between f_r and $2f_r$. The emergence of the first PD was indicated to be enhanced by the presence of noise, especially when the excitation frequency was approximately two times that of the relaxation frequency. The PD was confirmed to have a virtual Hopf precursor. The predictions were satisfactorily confirmed by experiment on an InGaAsP DFB laser at 1.55 μm. It was concluded that virtual Hopf precursor for period doubling was understood to be the persistent property in the current injection semiconductor laser. All the relevant results in the observed work might provide a key of quantitative reference for most practical applications.

References

[1] J. P. Eckmann, "Roads to turbulence in dissipative dynamical systems," *Rev. Mod. Phys.*, vol. 53, pp. 643–654, Oct. 1981.

[2] J. Sacher, D. Baums, P. Panknin, W. Elsasser, and E. O. Gobel, "Intensity instabilities of semiconductor lasers under current modulation, external light injection, and delayed feedback," *Phys. Rev. A*, vol. 45, pp. 1893–1905, Feb. 1992.

[3] W. Harth, "Large-signal direct modulation of injection lasers," *Electron. Lett.*, vol. 9, pp. 532–533, Nov. 1973.

[4] S. Tarucha and K. Otsuka, "Response of semiconductor laser to deep sinusoidal injection current modulation," *IEEE J. Quantum Electron.*, vol. QE-17, pp. 810–816, May 1981.

[5] D. F. G. Gallagher, I. H. White, J. E. Carroll, and R. G. Plumb, "Gigabit Pulse position bistability in semiconductor lasers," *J. Lightwave Technol.*, vol. LT-5, pp. 1391–1398, Oct. 1987.

[6] R. S. Tucker and I. P. Kaminow, "High-frequency characteristics of directly modulated InGaAsP ridge waveguide and buried heterostructure lasers," *IEEE J. Lightwave Technol.*, vol. LT-2, pp. 385–393, Aug. 1984.
[7] C. H. Lee, T. H. Yoon, and S.Y. Shin, "Period doubling and chaos in a directly modulated laser diode," *Appl. Phys. Lett.*, vol. 46, pp. 95–97, Jan. 1985.
[8] Y. C. Chen, H. G. Winful, and J. M. Liu, "Subharmonic bifurcations and irregular pulsing behavior of modulated semiconductor lasers," *Appl. Phys. Lett.*, vol. 47, pp. 208–210, Aug. 1985.
[9] H. G. Winful, Y. C. Chen, and J. M. Liu, "Frequency locking, quasiperodicity, and chaos in modulated self-pulsing semiconductor lasers," *Appl. Phys. Lett.*, vol. 48, pp. 616–618, Mar. 1986.
[10] M. Tang and S. Wang, "Simulation studies of bifurcation and chaos in semiconductor lasers," *Appl. Phys. Lett.*, vol. 48, pp. 900–902, Apr. 1986.
[11] ——, "Simulation studies of the dynamic behavior of semiconductor lasers with Auger recombination," *Appl. Phys. Lett.*, vol. 50, pp. 1861–1863, June 1987.
[12] G. P. Agrawal, "Effects of gain nonlinearities on period doubling and chaos in directly modulated semiconductor lasers," *Appl. Phys. Lett.*, vol. 49, pp. 1013–1015, Oct. 1986.
[13] Y. Hori, H. Serizawa, and H. Sato, "Chaos in a directly modulated semiconductor laser," *J. Opt. Soc. Amer. B*, vol. 5, pp. 1128–1132, May 1988.
[14] N. H. Jensen, P. L. Christiansen, and O. Skovgaard, "On period doubling bifurcations in semiconductor lasers," *Proc. Inst. Elec. Eng.*, vol. 135, pt. J, no. 4, pp. 284–288, Aug. 1988.
[15] T. H. Yoon, C. H. Lee, and S. Y. Shin, "Perturbation analysis of bistability and period doubling bifurcations in directly-modulated laser diodes," *IEEE J. Quantum Electron.*, vol. 25, pp. 1993–2000, Sept. 1989.
[16] L. Chusseau, E. Hemery, and J. Lourtioz, "Period doubling in directly modulated InaAsP semiconductor lasers," *Appl. Phys. Lett.*, vol. 55, pp. 822–824, Aug. 1989.
[17] E. Hemery, L. Chusseau, and J. Lourtioz, "Dynamic behaviors of semiconductor lasers under strong sinusoidal current modulation: Modeling and experiments at 1.3 μm," *IEEE J. Quantum Electron.*, vol. 26, pp. 633–641, Apr. 1990.
[18] Y. H. Kao and H. T. Lin, "A study of harmonic distortions and period doubling in DFB ridge waveguide laser with strong current modulation," *Opt. Commun.*, vol. 88, pp. 415–418, Apr. 1992.
[19] J. Katz, S. Margalit, C. Harder, D. Wilt, and A. Yariv, "The intrinsic electrical equivalent circuit of a laser diode," *IEEE J. Quantum Electron.*, vol. QE-17, pp. 4–7, Jan. 1981.
[20] K. Wiensenfeld, "Virtual Hopf phenomena: A new precursor of period doubling bifurcations," *Phys. Rev. A*, vol. 32, pp. 1744–1751, Sept. 1985.
[21] Y. H. Kao, H. T. Lin, and C. S. Wang, "Noise enhancement of period doubling in strongly modulated semiconductor lasers," *Japan. J. Appl. Phys.*, vol. 31, p. 2, pp. L846–L849, July 1992.
[22] D. Marcuse, "Computer simulation of laser photon fluctuations: Theory of single-cavity laser," *IEEE J. Quantum Electron.*, vol. QE-20, pp. 1139–1148, Oct. 1984.
[23] T. S. Parker and L. O. Chua, *Practical Algorithms for Chaotic Systems*. New York: Springer-Verlag, 1989.
[24] Y. H. Kao, C. H. Tsai, and C. S. Wang, "Observations of bifurcation structure in a rf driven semiconductor laser using an electronic simulator," *Rev. Sci. Instrum.*, vol. 63, no. 1, pp. 75–79, Jan. 1992.

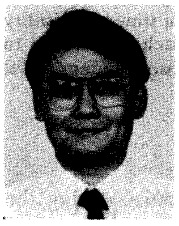

Yao Huang Kao (M'86) was born in Tainan, Taiwan, Republic of China, in 1953. He received the B.S., M.S. and Ph.D. degrees from National Chiao-Tung University in electronic engineering in 1975, 1977, and 1986, respectively.

Since 1986, he has been an associate Professor at department of communication engineering, National Chiao-Tung University, Hsinchu, Taiwan. He has also been a visiting scholar, working in nonlinear circuit, in University of California, Berkeley in 1988. His current research interests involve nonlinear dynamics and chaos, high speed optical communications, and microwave circuit designs.

Hung-Tser Lin was born in Taipei, Taiwan, Republic of China in 1967. He received his B.S. degree from Feng-Chia University, Tai-Chung, and the M.S. degree from National Chiao-Tung University, Hsinchu, in 1989 and 1991, respectively. He is now working toward the Ph.D. degree in the area of optical fiber communication at Chiao-Tung University.